PHYSICAL REVIEW B VOLUME 38, NUMBER 16 1 DECEMBER 1988

Long-wavelength sound propagation in superfluid-filled porous media with novel geometries

J. A. Roth,* T. P. Brosius, and J. D. Maynard
The Pennsylvania State University, University Park, Pennsylvania 16802
(Received 30 June 1988)

The acoustic-scattering corrections of several types of superleaks have been measured, providing information about inertial drag effects in the flow of superfluid ^{4}He. The porous media which have been studied include Al_2O_3 packed powder, Grafoil, and Grafoil foam. The frequency dependence of the acoustic-scattering correction was measured for the Grafoil media.

INTRODUCTION

Wave propagation and fluid flow in random media, classical areas once treated by Lord Rayleigh,[1,2] are currently receiving renewed activity. Reasons for the current interest involve practical applications, such as acoustic geophysical survey in porous rock, medical imaging, dielectric properties of granular composites, etc., and new basic research areas such as studies of fractal systems.[3,4] Wave propagation in these systems involves the physics of multiple scattering, an old and difficult but still very active area of research.[5,6] Modern theoretical techniques which have been directed toward this problem include percolation theories,[7,8] effective-medium theories,[8,9] fractal models,[4] Anderson localization theory,[10] etc. Although precise calculations for multiple scattering are difficult, some important results may be obtained by noting that a number of different phenomena associated with a particular random medium are governed (at least in some approximation) by the Laplace equation with complex boundary conditions determined by the random medium. While the equations are too difficult to solve in detail, the sharing of the equations by the different phenomena allows one to derive rigorous relationships among the various parameters of the different phenomena. For example, the multiple-scattering effects for long-wavelength sound propagation in a fluid-filled porous medium may be precisely related to the inertial drag experienced by the fluid when the porous medium is accelerated from rest.[11–15]

An important property of the random medium is its geometry, which may be characterized as randomly packed spheres, parallel plates, randomly oriented plates, parallel needles, randomly oriented needles, fractal, etc. While theoretical predictions for the various geometries are advancing,[5,16,17] experiments have tested only a few varieties: packed spheres,[18,19] random needles (chains of linked spheres),[19–21] and packed parallel plates.[22–24] In this paper we report experimental measurements on three different porous media with geometries approximating random needles (packed aluminum oxide powder, which forms chains of linked spheres), packed parallel plates (exfoliated graphite, Grafoil), and randomly oriented plates (Grafoil foam). For the packed powder medium both the acoustic scattering and the inertial drag were measured, and the failure of one of the rigorous theorems, which had been observed earlier,[12,13,25,26] was confirmed. Motivated by this result, we were able to discover an explanation for the discrepancy, which has been reported in an earlier paper.[15] The experiment with the Grafoil also confirmed other measurements,[22] but some discrepancies still need clarification. The Grafoil foam, which approximates randomly oriented plates with large open voids, is (acoustically) a new type of medium, and our measurements provide a significant amount of precise data for this new system. The data clearly indicates that more theoretical work, such as that initiated by Andrei and Glaberson,[22] is required. Current theory relevant to the experimental results reported here may be found in Ref. 15 and references cited therein; a brief review of the theory is provided below.

BRIEF DISCUSSION OF THEORY

When the wavelength of an excitation in a medium is considerably larger than an isolated scattering object, then the perturbation is weak and the scattering is easily calculated. However, the complexity of the problem changes dramatically when the medium contains a random distribution of objects which may interact through multiple scattering.[6] Many of the theories of multiple scattering are limited to the case of dilute scatterers,[6] but recent iterative techniques[27] have extended the range of validity closer to the percolation threshold of the wave medium. A particularly interesting and important case occurs when both the original wave medium and the scattering material are continuous and percolating, as in a fluid-saturated porous medium. For such a system two longitudinal acoustic modes are possible,[28] and this property can be used to invalidate many of the effective medium theories.[29] A valid phenomenological theory for a copercolating fluid-solid system which accounts for the motion of both components was introduced by Biot[28] and developed by Johnson and Sen,[13] and predictions with this theory have been experimentally verified in porous media consisting of fused glass spheres.[18] The Biot theory has two regimes determined by the viscosity of the fluid constituent. When the viscosity is high so that the fluid is limited to moving with the solid frame, then the validity of the effective medium theories for a viscoelastic material is recovered. The interesting (and most useful) acoustic properties occur when the fluid viscosity is low so that the fluid can move independently from the solid frame, thus allowing the propagation of the Biot slow

wave.[28] From the Biot theory the speed of propagation of long wavelength sound in a fluid filling a rigid porous frame is given by[11-14]

$$C = C_0/n \ , \tag{1}$$

where C_0 is the speed of sound in the pure fluid and the acoustic-scattering correction or index of refraction n is a parameter determined by the actual geometry of the frame. Using a self-similar replication theory, Sen, Scala, and Cohen[30] predict that

$$n = P^{(1-m)/2} \ , \tag{2}$$

where P is the porosity (open volume over total volume) of the frame and the exponent m depends on the generic geometry of the frame. For packed spheres and random needles m is $\frac{3}{2}$ and $\frac{5}{3}$, respectively. Packed Al_2O_3, commonly used as a superleak, appears to form chains of linked spheres which act as random needles, so that $n = P^{-1/3}$.[13]

For long-wavelength propagation and vanishing viscosity (i.e., an ideal Euler fluid) the motion of the fluid relative to the solid locally obeys the Laplace equation with appropriate boundary conditions at the solid walls. Through this boundary value problem, the acoustic properties of the fluid-filled porous medium may be related to a number of problems involving random media. In particular, the acoustic properties may be related to a continuous flow of the fluid through the porous medium.[11-14] When a foreign body moves at constant velocity through an ideal Euler fluid, there are no forces of interaction; there is no viscosity, no circulation can be created around the body, and the Euler fluid executes pure potential flow. However, if there is a relative acceleration then there is an effective hydrodynamic force referred to as inertial drag.[31] If a fluid-filled porous medium is accelerated from rest to a steady velocity V, a mass flow is induced in the fluid with an average velocity $V_i = \lambda V$.[19] Because the acoustic scattering and the induced flow are governed by the same boundary value problem in a given fluid-filled porous medium, one has the rigorous relation[11-13]

One way of measuring n and λ simultaneously is to use the Doppler shift of sound in the presence of the induced flow. For sound transducers moving with a porous medium at a velocity V (after being accelerated from rest) Bergman, Halperin, and Hohenberg[12] have shown that

$$C \pm \Delta C = \frac{1}{n} C_0 \pm (1-\lambda) V \ , \tag{4}$$

where $C \pm \Delta C$ are the sound speeds for propagation with and against the fluid flow relative to the medium. In order to avoid end-effect complications in a finite experimental system, one may use a porous medium in a large diameter annular channel where the fluid is induced to flow circumferentially around the annulus when the ring is brought from rest to rotation about the symmetry axis perpendicular to the plane of the annulus. If one assumes that the channel width is much smaller than the diameter of the ring, and if one applies Eq. (4) in the usual manner,[25,26] then one finds that the fundamental acoustic resonance frequencies of the annulus ($f_0 \pm \Delta f$) are given by

$$f_0 \pm \Delta f = \frac{1}{n} \frac{C_0}{L} \pm (1-\lambda)\Omega \ , \tag{5}$$

where L is the mean circumference of the annulus and $\Omega = V/L$ is the rotation rate after acceleration from rest.

Superfluid ^{4}He in an annular superleak fourth-sound resonator[25,26] at low temperatures (or with thermodynamic corrections at higher temperatures[11,12]) accurately satisfies the conditions leading to Eq. (5). Modifications to Eq. (5) due to subtle acoustic properties of an annular resonator are discussed in Ref. 15. For the purpose of analyzing the experimental results in this paper, Eq. (5) is sufficiently accurate to provide the means for determining n and λ from acoustic Doppler shift measurements.

EXPERIMENTAL APPARATUS AND PROCEDURES

General features

The major features of the cryostat system are a large-diameter Dewar which permits the rotation of large resonators for high linear fluid velocities, external equipment platforms that permit rotation of detection instruments along with the experimental apparatus, and quick coupling between the cryostat insert and the external components for easy access to the experiment. An overall view of the cryostat insert is given in Fig. 1. Two degreased bearings provide alignment and smooth rotation of the main shaft. The experimental cell, consisting of annular acoustic resonators, is attached to the bottom flange. All wiring and plumbing connections to the experimental cell pass through the main shaft. Other features involve standard cryogenic techniques.

The cryostat insert is connected through a flexible coupling to a rotating superstructure mounted above the Dewar; this superstructure and its support frame are shown in Fig. 2. The rotational motion from the drive mechanism is transmitted to the cryostat insert by bolting two flanges together. The upper flange is attached to the main shaft of the rotating superstructure by a phosphor-bronze bellows which allows for slight misalignment of the upper rotating axis and the cryostat insert axis, as well as providing a vacuum-sealed coupling. The components of the superstructure consist of the rotating-shaft vacuum seal, the vacuum feedthroughs at the termination of the main shaft, the equipment platforms, the commutator assembly, and the drive mechanism. The motor and drive chain mechanisms are mounted between the middle structural bulkhead and a secondary aluminum plate, just below the equipment platforms. The motor system is a Servo Translator manufactured by CSR, Inc.;[32] a maximum motor shaft velocity of 600 rpm may be achieved. The manufacturer's specifications state the speed accuracy to be one part in 10^4. A problem inherent in conventional gear or chain drives is backlash caused by the clearances

necessary to permit smooth engagement, and with chain drives some method must be provided to adjust the tension in the chain. A patented drive chain system, Flex-E-Gear, manufactured by Winfred M. Berg, Inc.[33] solves the backlash problem, and a floating pivot mount allows the tension to be adjusted with few additional components to the mechanism. With a 10:1 reduction the maximum rotation speed of the cryostat insert is ~ 1 revolution per second. Accelerometer measurements made at the bottom flange of the cryostat insert show no evidence of any irregularities or resonances in the drive mechanism, nor any evidence of the pulsed nature of the motor drive. The high moment of inertia of the rotating cryostat serves to mask most fluctuations in the motion.

EXPERIMENTAL CELL

One of the primary goals of this experimental investigation is a comparison of the propagation of fourth sound in a typical superleak (compacted Al_2O_3 powder) with the propagation in several Grafoil superleaks. The easiest way to make this comparison is by making simultaneous measurements on two superleaks. For this reason, a double resonator, illustrated in Fig. 3, was constructed. Concentric annuli contain the two superleaks, and a small diameter capillary connects the two resonator chambers together. This assembly ensures identical pressures and temperatures at all times for the different superleaks. Fourth-sound resonances are excited and detected by using any of four identical transducers on each resonator. The experimental cell is made in two sections: a lower half containing the superleaks, and an upper half in which the transducers are mounted (see Fig. 3). Four grooves are cut into the lower half of the cell, concentric with the annuli, one just to the outside and

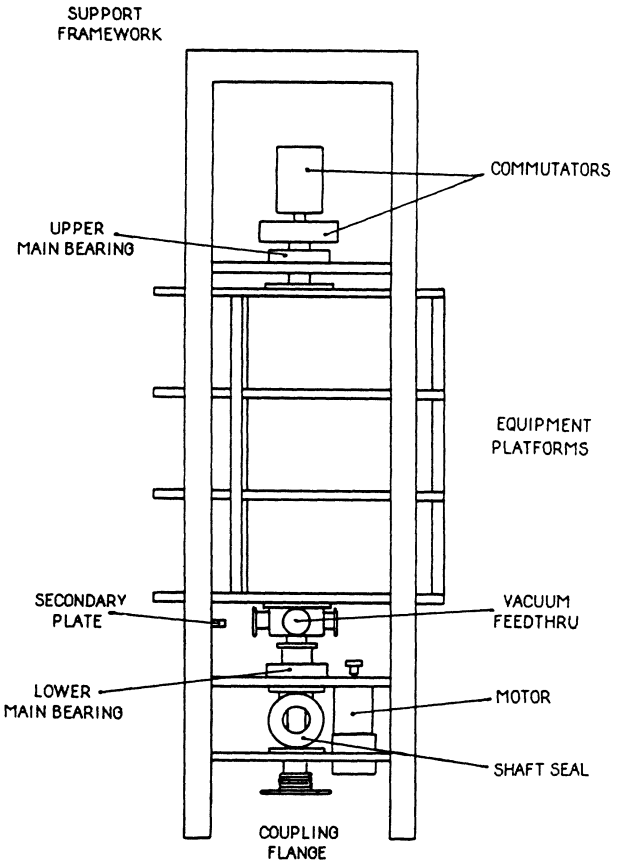

FIG. 2. Rotating cryostat superstructure and support frame.

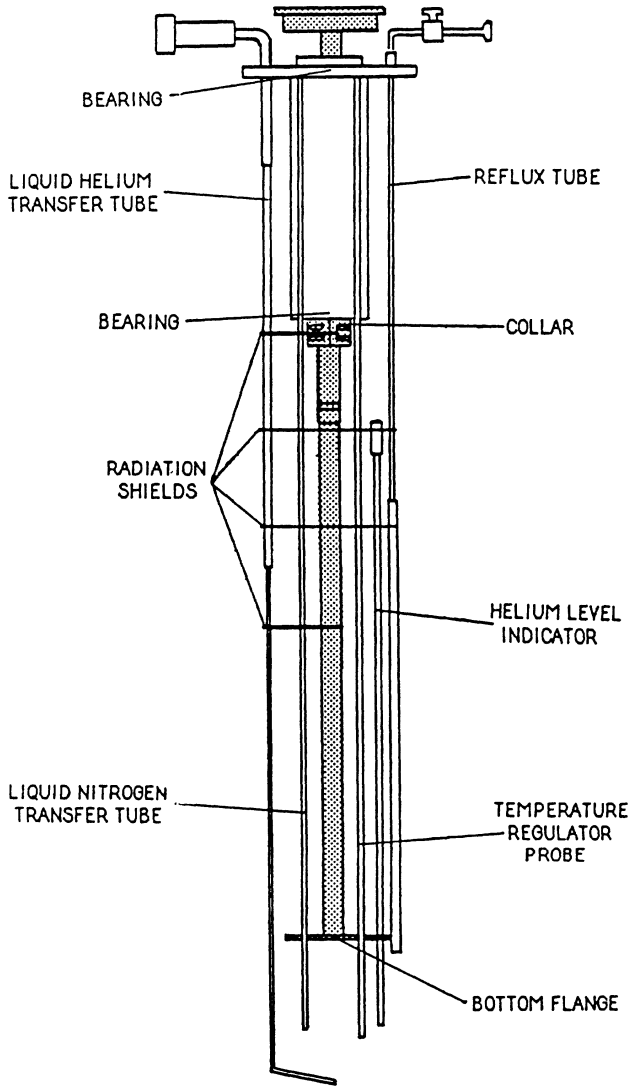

FIG. 1. Rotating cryostat insert.

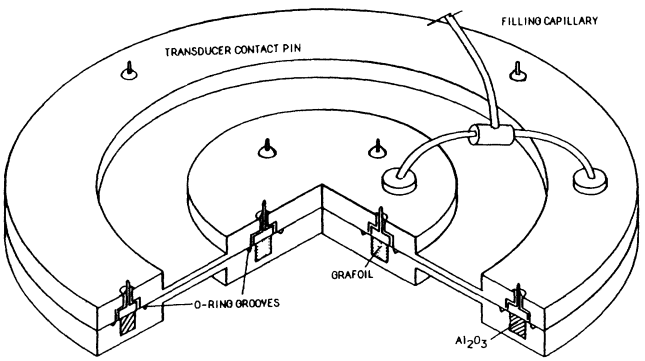

FIG. 3. Double annular acoustic resonators.

one just to the inside of each resonator chamber. Into these grooves are placed O rings formed from indium metal, which under the compression from the 96 8-32 screws bolting the halves of the cell together, completely seal the cell. The filling capillary connects to each resonator chamber via a flange that seals with its own indium O ring. The filling capillaries join at a "Y" connector before connecting to the external gas supply through a capillary in the cryostat insert. Stainless steel was used for the lower half of the cell due to the large forces involved during the process of compacting the Al_2O_3 powder. The volume of each resonator chamber is completely contained within the lower half of the cell. The cross sections of the resonator chambers are identical: 6.4 mm square. The mean radius of the inner chamber is 2.22 cm and the mean radius of the outer chamber is 7.62 cm. These values were chosen to exactly fit the largest Grafoil sample available in the laboratory (for the inner chamber) and to have the largest resonator that would fit in the Dewar (for the outer chamber). The Grafoil sample is a semirigid ring designed to be an industrial shaft bushing.[34] The Al_2O_3 powder compacted into the outer resonator chamber is a nominal 0.05-μm polishing compound.[35] Electron micrographs made at the University of California–Los Angeles of an identical powder show an actual distribution of particle sizes from 0.0175 to 0.3 μm.[21] The powder was compacted into the chamber using a hand-operated hydraulic press along with a piston-and-sleeve assembly that bolts to the lower half of the cell. The Grafoil foam sample was cut from flat sheet stock provided by Union Carbide Corporation[34] to exactly fit the inner resonator chamber.

Transducers

The eight fourth-sound transducers of the experimental cell are all electret-type pressure detectors and/or generators. A charged diaphragm is one plate of a capacitor and an electrically isolated button in the upper half of the cell is the other plane. The diaphragms are 1-cm diam. disks cut from a sheet of 12.5-μm thick Teflon. Prior to cutting out the disks, a ~200-nm thick aluminum film is applied to one side of the sheet, using a vacuum-deposition system. After the disks are cut, they are charged in an 8-kV electric field for several hours. This traps charges within the molecular structure of the Teflon so that an external dc biasing voltage is not required for the operation of the transducers. Before assembling the cell, the exposed surface of the button is roughened with a sand blaster to enhance the compliance of the diaphragm which is placed over it. If the diaphragm is sufficiently charged it will be drawn down to the transducer button, and the button roughness will be evident at the surface of the diaphragm. The transducer can be tested at this time by applying a signal within the audible spectrum across it. A piece of indium wire is used to make contact with the diaphragm so as not to damage it. If the transducer is working correctly, a faint tone can be heard.

At the frequencies at which these transducers are operated during the course of this investigation (500–30 kHz), they have an impedance as high as 10^9 Ω. This presents several problems: difficulty in driving the signal cable load by a detector transducer, and susceptibility to noise generated in the Teflon insulated coax cables within the cryostat insert. For transducers used as sound detectors, both problems are overcome by using a metal-oxide–semiconductor field-effect transistor (MOSFET) impedance converter operating within the liquid helium bath, mounted as close as possible to the detector transducer.

Gas handling system

The gas-handling system used for the investigations of this report is straightforward, but has a few features worth discussing. A schematic of the system is given in Fig. 4. A length of small-diameter stainless steel capillary connects the resonators to a valve mounted to the lowermost rotating equipment platform. A short length of tubing soldered to the other side of the valve terminates in a soft-solderable connector. When it is time to rotate the cryostat, the valve is closed and this connection unsoldered. At other times, the gas handling system is constantly monitoring the resonator pressure. From this connector, tubing proceeds on to the main control panel of the system, which contains valves for venting the system, evacuating the resonators with a vacuum pump connected to the system, and pressurizing the resonators. A high-pressure commercial-grade-purity helium cylinder serves as the gas supply, buffered by a 1-l metering volume. A copper high-pressure bomb, inserted into a liquid-helium storage Dewar, is used to purify the helium gas before adding it to the resonators.

Temperature measurement and regulation

The primary temperature standard used in this system, for temperatures at and below the normal boiling point of helium, is based on the 1958 ^{4}He vapor pressure standard. The secondary temperature standard is a commercial germanium resistance thermometer, which is calibrated against the vapor pressure readings, and therefore serves as the sensor for the liquid-helium bath temperature regulation system. The regulation is accomplished with the standard ratio transformer bridge and feedback system.

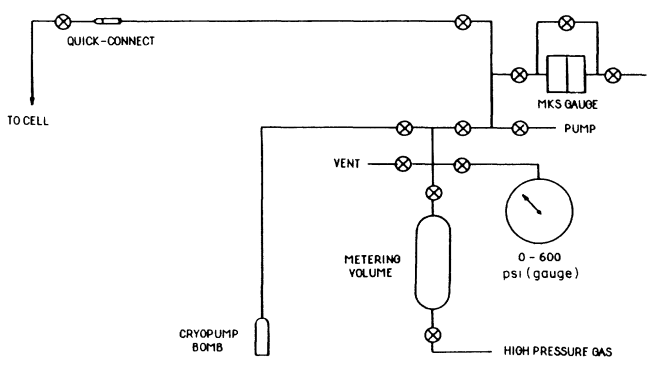

FIG. 4. Gas-handling system.

Operating procedures

Two techniques have been employed in the study of persistent currents and pure potential flow states: cooling down below the λ point while rotating, and rotating after having cooled. The first method was most frequently used. After liquid-helium transfer, and when the ^{4}He vapor pressure reaches 0.1 bar, the motor is powered up, and the rotation speed is smoothly increased to the desired rate. A vapor booster pump is then put on line to more rapidly cool everything down to the operating temperature. This rotating while cooling down through the λ point produces a persistent superfluid current in the superleaks, as viewed from the laboratory reference frame. In this way, Doppler shift measurements can be made with the cryostat stationary, a simpler task than making measurements while it is rotating. After the cryostat has reached the desired temperature, the rotation is smoothly stopped, and the gas handling system is reconnected. The resonator chamber pressure is then adjusted to be the saturated vapor pressure for the current temperature, and fourth-sound observations are made. Should measurements need to be made while the cryostat is rotating, the Dewar is immediately cooled down to the operating temperature. Initially, the cell is pressurized to several bars, and then the pressure is reduced to the saturated vapor pressure; this ensures no trapped gas forms pockets in the superleaks. Once the desired operating pressure is reached, the gas-handling system is disconnected, the cryostat rotated, and fourth-sound observations are made.

Whether the persistent current exists from the superfluid component of the He II being in motion in the laboratory reference frame, or by the superleak (and thus the normal fluid component) being in motion in the laboratory reference frame, the Doppler-shift measurements are made in the same manner. The actual quantities measured are the harmonics of the resonant frequencies of the annular resonators. For the jth harmonic resonant frequency f_j ($j=1,2,\ldots$),

$$f_j = jC_4/nL \ , \tag{6}$$

where n is the acoustic scattering correction for the superleak,[12–14] L is the mean circumference of the annulus, and C_4 the (tabulated) velocity of fourth sound. Verification that observed signals are in fact fourth sound is made by noting the changes in the resonant frequency as the temperature and pressure are varied.

EXPERIMENTS

This section presents the measurements made for each of the three different superleaks. The data taken and the analysis done for each system will be presented in individual sections. Since the examination of the Al_2O_3 packed-powder superleak additionally served as a reference for the subsequent work on the two Grafoil superleaks, the results for that system will be covered first. The next sections discuss, in order, the Grafoil superleak and the Grafoil foam superleak.

Aluminum oxide packed powder

Utilizing the large-diameter, small-cross-section annular resonator, packed with nominal 0.05-μm Al_2O_3 powder, measurements of the Doppler splitting have been made for both methods of establishing a persistent current. Also measured were the wave velocity as a function of temperature and pressure, and the velocity of the fundamental "depth" mode of the system.

From several harmonic resonance frequencies, using Eq. (6), we obtain an average value for the acoustic scattering correction $n=1.12\pm0.01$, where the uncertainty is twice the standard deviation of the averaged values. The measured porosity for the packed powder was $P=0.77\pm0.01$. From the theoretical relation[13] for chains of linked spheres (randomly aligned needles) $n=P^{-1/3}$, we would have $n=1.09\pm0.01$, which is in reasonable agreement with the actual value of n. These results are very close to those found by Kojima *et al.*[26] using a similar superleak.

Extensive measurements of the pressure and temperature dependence of the sound speed were not made here, having been studied in detail by others.[20,25,26] Instead, these measurements were used to establish that the observed sound was in fact fourth sound. The lack of any systematic variation with pressure or temperature in the scattering corrections, determined as fitting parameters, has been taken as positive confirmation.

The saturated persistent current velocity has a temperature dependence that matches the superfluid fraction ρ_s/ρ. Once a persistent current has been established, the maximum velocity it can maintain depends upon its historical highest temperature. If the persistent current established in the Al_2O_3 superleak is within the reversible Landau region, a temperature quite close to T_λ must be reached in order to decrease the velocity. Figure 5 shows four plots of the 24th harmonic of the fundamental circumferential resonance. A persistent current was established in the superleak by rotating the cryostat while cooling down to 1.45 K. At that temperature, the system was brought to rest and plot (a) was made. The system was warmed to 1.95 K, then cooled back down to 1.45 K at which time the plot (b) was made. This procedure was repeated twice more, with maximum temperature of first 2.05 K and then 2.10 K. No decrease in the splitting, and hence the persistent current velocity, was observable until the system had been warmed to 2.10 K. This procedure was repeated several times over the course of months that the experiment was being conducted, with no variations in observed behavior. That a temperature within 72 mK of T_λ was necessary to decrease the persistent current velocity is strong evidence that the velocity is far from critical and within the Landau region. The persistent current established for the plots in Fig. 5 is the fastest one possible with the particular gearing of the rotating cryostat, corresponding to a rotation rate of 1 rps and a linear velocity at the mean radius of the superleak of 49 cm/s. All four plots were made at the same temperature to permit a direct comparison of the splitting, without having to actually calculate the superfluid velocity.

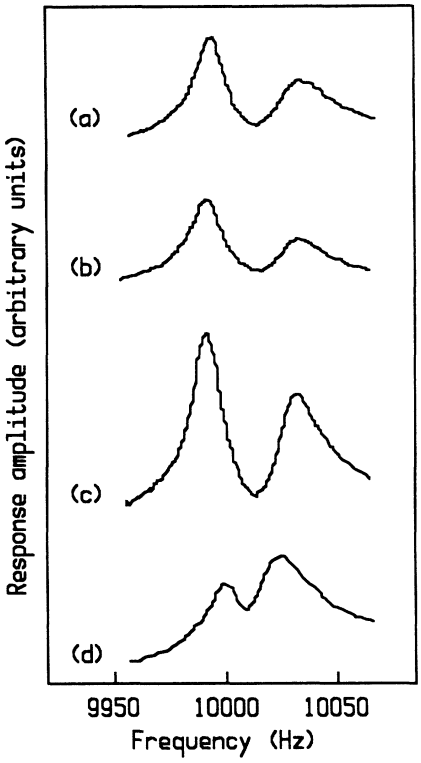

FIG. 5. Doppler splitting in the 0.05-μm aluminum oxide superleak as a function of historical temperature. (a) Splitting after rotating while cooling to 1.45 K. (b) Splitting after warming to 1.95 K and recooling. (c) Splitting after warming to 2.05 K and recooling. (d) Splitting after warming to 2.10 K and recooling.

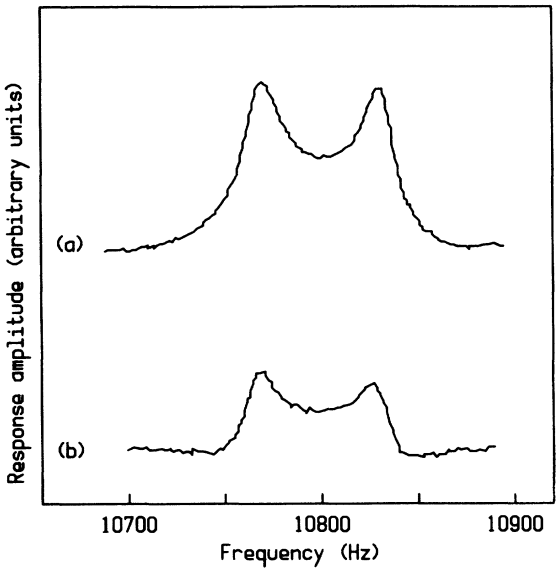

FIG. 6. Comparison of Doppler splitting in the 0.05-μm aluminum oxide superleak from the two methods of establishing a persistent current. (a) Rotating, cooling through T_λ, decelerating to test, then measuring. (b) Cooling through T_λ, accelerating into rotation, then measuring while rotating.

The measurements of interest for this system were made on persistent currents established by rotating the superleak after cooling down to the desired temperature. These measurements consist of the observed splitting as a function of rotational velocity. The other technique of establishing a persistent current, rotating after cooling, should give the same results. Such behavior is verified in Fig. 6. The upper plot was made after the cryostat had been cooled while rotating at maximum speed, while the lower plot was made at low temperature with the cryostat rotating at maximum speed. The peak-shape differences are due to the optimized instrument settings employed for each situation. The small deviation in observed splitting is in the direction expected, since the upper plot was made at a slightly lower temperature. The method of making measurements during rotation was used for the sequence of splitting versus rotational velocity in order to keep from making repeated cyclings of the system from above T_λ down to the operating temperature.

Some of the harmonics of the resonator exhibited the behavior discussed in Ref. 15: splitting due to effects other than the persistent current. These splittings are thought to be due to defects in the superleak. This necessitated careful selection of the harmonics for measurement. For the measurements made while rotating, the 33rd and 31st harmonics were observed. The 24th and 26th harmonics were followed for persistent currents established by cooling while rotating.

At low temperatures the expression for the Doppler splitting Δf_j of the jth harmonic frequency due to the superfluid flow in the annular channel is

$$\Delta f_j = 2j(\rho_s/\rho)V_s/L \ , \tag{7}$$

where ρ_s/ρ is the superfluid fraction, L is the mean circumference of the annulus, and V_s is the velocity of the superfluid relative to the superleak after the superleak has been accelerated (or decelerated) through a circumferential velocity change V. A plot of V_s determined from two different harmonics at a temperature of 1.45 K for various values of V is shown in Fig. 7; the circles are for the 31st harmonic and the triangles for the 33rd har-

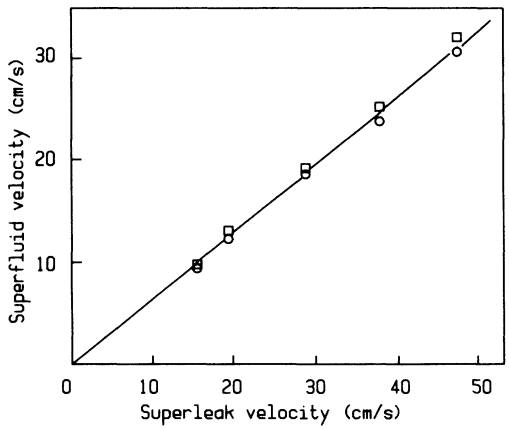

FIG. 7. Relative superfluid velocity vs superleak velocity for the 0.05-μm aluminum oxide superleak at a temperature of 1.45 K. Circles are for the 31st harmonic and squares are for the 33rd harmonic.

monic. The error bars that are associated with these points are ±0.5 cm/s. The large percentage uncertainty is due to the fact that Δf_j is the difference between two large numbers, which in turn depend on precisely determining the center of each peak. It is reassuring to note that a reasonable straight line, passing through zero, can be drawn through the data points, as should be the case for data in the Landau region. Figure 8 shows the progression of the splitting for the 33rd harmonic from at rest (and never rotated) up to maximum rotational speed. The reversibility of the system over the range of rotation rates used was checked by bringing the system to a halt before each successive higher-speed run. This is amply illustrated by Fig. 9. Plot (*a*) is the 33rd harmonic with the system never having been rotated, plot (*b*) is the same harmonic with the system again at maximum speed, and plot (*c*) is the harmonic with the system again at rest, after the high-speed rotation. Only 6 min elapsed between plot (*b*) and the first plot of the sequence containing plot (*c*).

Figure 9 illustrates the typical quality factor (Q) in these experiments, which is about 1000–2000. Better fourth-sound Q's of about 10 000 can be obtained, but this requires lower temperatures and, most importantly, a carefully sealed resonator. The Q's which we obtained are typical for our resonator design.[36]

According to the theory of Bergman *et al.*[12] one should have $V_s=(1/n^2)V$. The slope of the line fitting the data in Fig. 7 (and passing through the origin) is 0.64, which agrees very well with the earlier data of Kojima *et al.*[26] for a similar superleak. However, this differs significantly from the value of $1/n^2=0.80$; the discrepancy of ~20% is well outside the precision of the measurement, and represents a serious failure of the theory. Motivated by this result we have reexamined the theory and have found that the original theory as derived is valid and the discrepancy results from subtle acoustic properties of an annular resonator. Details of this work have been published elsewhere;[15] for the purposes of this paper it is sufficient to note that the results with the Al_2O_3 superleak are very consistent (agreeing well with the results of Kojima *et al.*) and that for a complicated superleak (such as the Grafoil samples) in an annular resonator the value of V_s may be considerably less than $(1/n^2)V$.

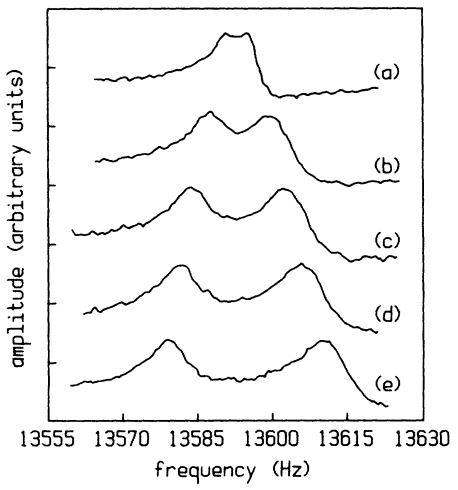

FIG. 8. Doppler splitting of the 33rd harmonic in the 0.05-μm aluminum oxide superleak at a temperature of 1.45 K as a function of cryostat rotational speed. The various circumferential speeds are (a) 16 cm/s, (b) 20 cm/s, (c) 30 cm/s, (d) 40 cm/s, and (e) 50 cm/s.

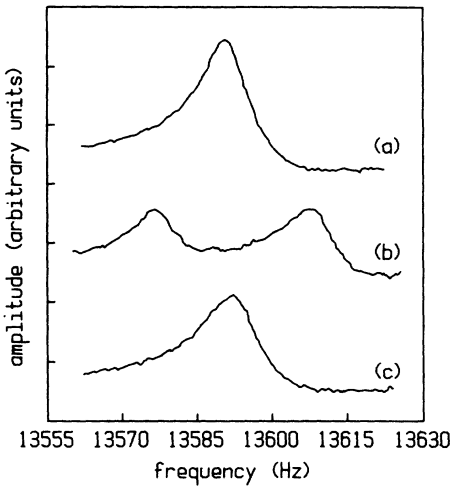

FIG. 9. Plots of the 33rd harmonic in the 0.05-μm aluminum oxide superleak at 1.45 K demonstrating the reversibility of the Doppler splitting. (a) System at rest, never having been rotated. (b) System at 50 cm/s. (c) System returned to rest after rotation.

Grafoil

For the Grafoil sample, a comparison of the measured fourth-sound speed and the theoretical (tabulated) C_0 yields a constant value for the scattering correction $n=4.40\pm0.05$ at all temperatures and pressures. Using this value of n in Eq. (2) and the value $P=0.43$ for Grafoil, we find $m=4.5$. In other Grafoil samples we have found scattering corrections of 6.5 (Ref. 23) and ~8, and Andrei and Glaberson[22] have reported values of $n\sim18$. Since the Grafoil sample porosities are approximately the same, such variations in n (and m) cannot be accounted for in the Biot theory; extensions of the theory as suggested by Anderi and Glaberson[22] and by Maynard[15] are indicated.

From the result $V_s<(1/n^2)V$ and the large value of n for Grafoil, it is expected that there will be only a very small motion of the superfluid relative to the superleak; most of the superfluid will be brought into motion with the superleak by the large inertial drag. Using Eq. (3) and $n=5$, one finds that the expected frequency splitting would be less than 0.01 Hz, which would be too small to detect; the typical width of the resonance peaks for the Grafoil is ~1 Hz. To check this upper limit, a Doppler-shift measurement similar to those described for the Al_2O_3 superleak was performed for the Grafoil superleak. Figure 10 shows plots of the fourth harmonic with plot (*a*) made immediately after stopping a full speed rotation initiated while the system was still above T_λ and plot (*b*) made after warming. Clearly, no substantial difference is

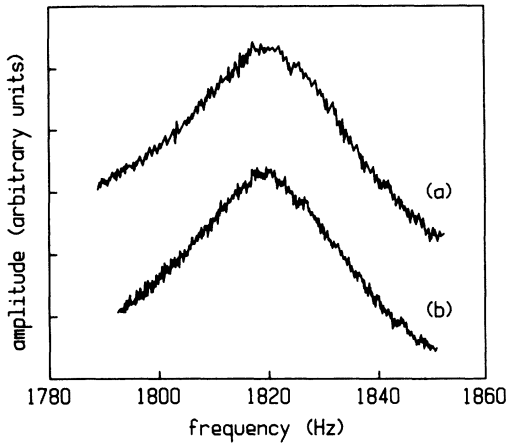

FIG. 10. A resonance peak in the Grafoil resonator at 1.45 K (a) with and (b) without rotation. The Doppler splitting is immeasurably small.

detectable, which is consistent with the anticipated value of the Doppler shift.

Typical frequency plots obtained with the Grafoil superleak are shown in Fig. 11. The measurements were made with both of the source and/or detector transducer pairs. Which pair was used for any particular data run depended upon which MOSFET impedance converter was working better at that time. The "depth" mode onset was also measured for this superleak, but discussion of this will be reserved until the end of this section.

Grafoil foam

Upon completion of the measurements with the Grafoil superleak, a Grafoil foam sample was procured from Union Carbide[34] for investigation. Work done on third sound in a Grafoil foam superleak suggested this system might have a smaller scattering correction which would permit observations of fourth-sound Doppler-splitting due to a superfluid flow. The porosity of this material is 0.95, considerably different from Grafoil. The Grafoil foam sample did indeed provide a superleak with a smaller scattering correction than the Grafoil superleak, but for several reasons it was not suitable for superfluid flow Doppler shift measurements. The pore size in the superleak was not small enough to viscously clamp the normal fluid, resulting in the propagation of first sound. Evidence of this is presented by Fig. 12(a) which was made during the liquid-helium transfer, i.e., at 4.2 K; for comparison, Fig. 12(b) was made at 2.13 K. The similar features must be due to first sound. This effect by itself does not eliminate the possibility of Doppler-shift measurements since at low enough temperatures first- and fourth-sound modes are the same. The effect does result in a complicated resonator frequency spectrum, as shown in Fig. 13.

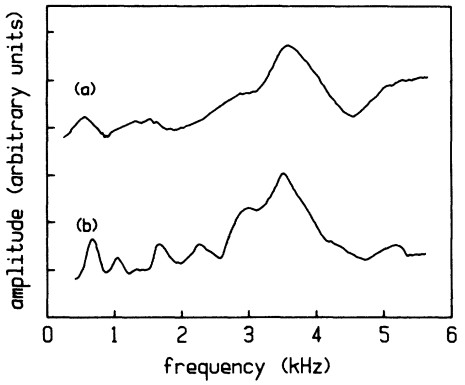

FIG. 12. Evidence of the propagation of ordinary sound in the Grafoil foam porous material. (a) Acoustic spectrum above the λ transition. (b) Acoustic spectrum at 2.13 K.

The Grafoil foam data showed a number of interesting features, which are discussed individually below. Because the data were taken at discrete temperatures, pressures, harmonic numbers, etc., and the data cannot be described in terms of the fundamental sound modes of helium, the data is presented in tabular form (in Tables I–IV). In order to remove much of the pressure dependence, etc., the data are normalized with the velocity of first sound; i.e., the data is presented as an effective acoustic scattering correction, $n = C_0/C$ where C_0 is the known velocity of first sound at the temperature and pressure where C was measured. Rather than being a constant, as was found for the other superleaks studied,

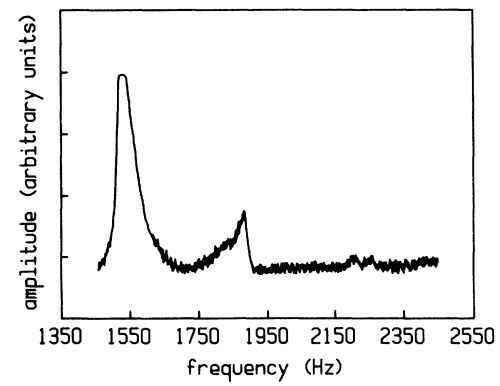

FIG. 11. Typical acoustic spectrum of the Grafoil superleak at a temperature of 1.45 K, showing the fourth, fifth, and sixth harmonics.

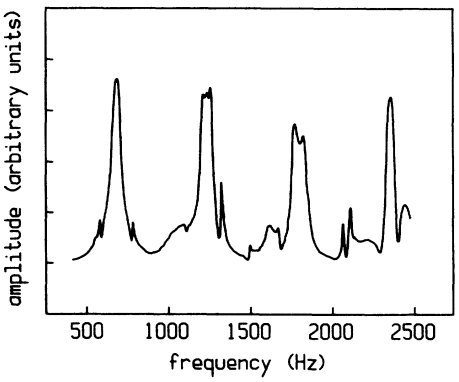

FIG. 13. Complex acoustic spectrum of the Grafoil foam at 1.6 K.

TABLE I. Grafoil foam scattering correction, first data run, first transducer pair for various temperatures and pressures. The individual values of n are calculated for each indicated harmonic, whose actual resonance frequency is given in parentheses. A pressure value of 0 indicates saturated vapor pressure. Missing values indicate that the center frequency was obscured.

			Scattering correction n (Resonance frequency) (Hz)					
T (K)	P (bar)	Harmonic:	1	2	3	4	5	6
1.48	0			2.72	2.80	2.83	2.94	3.04
				(1242)	(1809)	(2384)	(2870)	(3348)
1.58	0		2.45	2.75	2.78	2.84	2.96	3.03
			(685)	(1220)	(1804)	(2364)	(2830)	(3324)
1.71	0		2.45	2.87	2.79	2.85	2.98	3.06
			(680)	(1160)	(1788)	(2340)	(2795)	(3264)
1.81	0		2.44	2.87	2.84	2.87	3.01	3.05
			(677)	(1154)	(1749)	(2304)	(2750)	(3252)
1.89	0		2.50	2.85	2.83	2.89	3.01	3.07
			(657)	(1152)	(1740)	(2272)	(2725)	(3210)
2.04	0			2.94	2.83	2.90	2.90	3.08
				(1094)	(1702)	(1707)	(2216)	(3610)
1.47	0		2.45	2.69	2.78	2.83	2.93	3.02
			(688)	(1252)	(1821)	(2388)	(2875)	(3348)
1.48	3.2		2.45	2.80	2.82	2.87	3.01	3.13
			(758)	(1328)	(1974)	(2588)	(3085)	(3558)
1.48	2.0		2.46	2.76	2.79	2.87		3.09
			(734)	(1302)	(1935)	(2508)		(3492)
1.48	1.4		2.46	2.76	2.79	2.86		3.08
			(717)	(1280)	(1902)	(2472)		(3444)

TABLE II. Grafoil foam scattering correction, first data run, second transducer pair for various temperatures and pressures. The individual values of n are calculated for each indicated harmonic, whose actual resonance frequency is given in parentheses. A pressure value of 0 indicates saturated vapor pressure. Missing values indicate that the center frequency was obscured.

			Scattering correction n (Resonance frequency) (Hz)			
T (K)	P (bar)	Harmonic:	1	2	3	4
1.45	0		2.45	2.71	2.78	2.87
			(688)	(1246)	(1818)	(2352)
1.88	0		2.53	2.83	2.95	2.93
			(649)	(1162)	(1671)	(2244)
2.13	0			3.06	3.53	3.85
				(1032)	(1341)	(1640)
1.48	0		2.48	2.83	2.87	2.90
			(679)	(1194)	(1764)	(2328)

TABLE III. Grafoil foam scattering correction, second data run, first transducer pair for various temperatures and pressures. The individual values of n are calculated for each indicated harmonic, whose actual resonance frequency is given in parentheses. A pressure value of 0 indicates saturated vapor pressure. Missing values indicate that the center frequency was obscured.

			Scattering correction n (Resonance frequency) (Hz)					
T (K)	P (bar)	Harmonic:	1	2	3	4	5	6
1.45	0		2.11	2.41	2.45	2.49	2.61	2.80
			(800)	(1400)	(2064)	(2716)	(3230)	(3618)
1.44	0		2.07	2.41	2.47	2.48	2.58	2.79
			(816)	(1402)	(2052)	(2720)	(3265)	(3636)

TABLE IV. Grafoil foam scattering correction, second data run, second transducer pair for various temperatures and pressures. The individual values of n are calculated for each indicated harmonic, whose actual resonance frequency is given in parentheses. A pressure value of 0 indicates saturated vapor pressure. Missing values indicate that the center frequency was obscured.

			Scattering correction n (Resonance frequency) (Hz)			
T (K)	P (bar)	Harmonic:	1	2	3	4
1.46	0		2.12 (795)	2.37 (1424)	2.46 (2058)	2.53 (2668)
1.48	1.2		2.13 (824)	2.40 (1460)	2.49 (2112)	2.60 (2704)
1.48	2.2		2.16 (837)	2.4 (1506)	2.5 (2175)	2.57 (2812)
1.48	3.0		2.19 (844)	2.43 (1518)	2.50 (2223)	2.58 (2864)
1.48	3.9		2.17 (870)	2.43 (1556)	2.58 (2205)	
1.48	4.7		2.18 (884)	2.44 (1578)	2.54 (2280)	
1.48	6.4		2.10 (954)	2.37 (1686)		
1.48	8.1		2.12 (977)	2.37 (1744)		
1.48	10.3		2.11 (1017)	2.45 (1750)		
1.48	12.0		2.12 (1042)	2.46 (1792)		
1.48	13.7		2.12 (1066)	2.49 (1814)		
1.48	15.7		2.15 (1081)	2.53 (1834)		

the Grafoil foam scattering correction shows frequency dependence and other artifacts, as will now be discussed.

The most interesting and significant behavior of the sound in the Grafoil foam is the dependence on harmonic number or frequency. For large pores one would expect frequency dependence for the following reason: as the frequency is increased, the viscous penetration depth decreases, the mode of propagation for the sound shifts from fourth sound toward first sound, and the scattering correction would decrease. However, the data in Tables I–IV indicate that the scattering correction instead increases with frequency. It is likely that this behavior is due to dynamic effects, involving compression of the fluid inside blind passages of the foam, etc., instead of the assumed incompressible flow of the standard theory. A major thrust of this paper is to have the measured frequency dependence of the sound in the Grafoil foam motivate the development of an improved theory for sound propagation in porous media.

Another interesting feature of the Grafoil foam data is the variation in the resonance spectrum which resulted from using the two different pairs of transducers, which were located at positions rotated 90° from one another. This may be explained by the Grafoil foam superleak not being completely homogeneous (i.e., not completely invariant under rotations), at least in a dynamical or acoustic sense. This possibility is consistent with the explanation of the inertial drag paradox for annular resonators, as discussed in Ref. 14.

Another artifact which should be explained is the change in the resonant frequency spectrum for the two isolated runs of the experiment on the same sample. A likely explanation arises from the fact that the Grafoil foam superleak is not packed, and the material is "soft," i.e., it does not have the mechanical integrity of the other packed superleaks. During the first run it is possible that

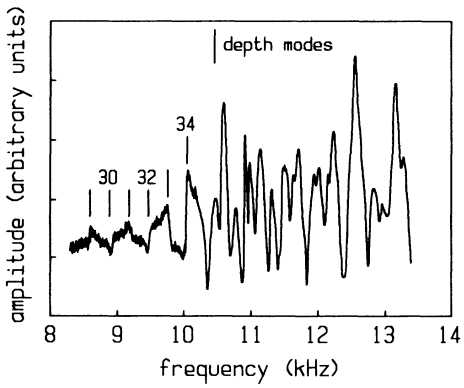

FIG. 14. Acoustic spectrum for the aluminum oxide superleak showing the circumferential harmonics 29–34, followed by the depth mode resonances.

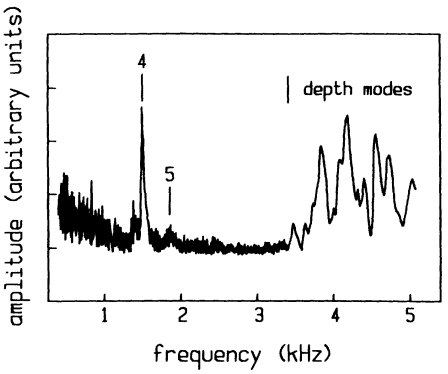

FIG. 15. Acoustic spectrum of the Grafoil superleak at 1.45 K with marks showing the fourth and fifth circumferential harmonics and the onset of the depth modes.

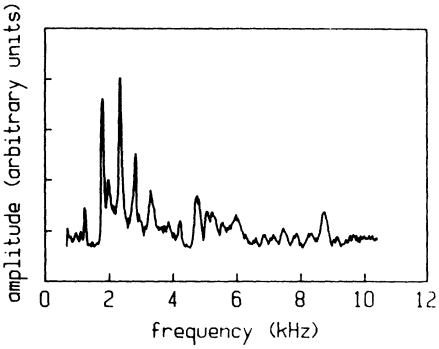

FIG. 16. Acoustic spectrum of the Grafoil foam porous material showing no distinct evidence of depth modes.

the pressurized superfluid became trapped in voids in the Grafoil foam which, upon warming to room temperature, caused a significant change in the geometry of the superleak. The change in actual geometry would result in a different scattering correction in the second run. Such a dependence on geometry details, rather than basic geometry and porosity, is consistent with the ideas discussed in Ref. 14.

Depth modes of the resonators

The principal harmonics studied have been of the circumferential resonances. These of course, due to the orientation of the superleaks, are the only ones that could exhibit Doppler splitting. However, by examining the depth modes of the annular resonators (corresponding to fitting an integral number of half wavelengths in the depth of the superleak channel), certain features are present that further characterize the propagation of sound in the system. Figure 14 shows the acoustic spectrum of the Al_2O_3 superleak at a high temperature. At this temperature the fourth-sound velocity has been reduced so that the frequency corresponding to the fitting of a half-wavelength along the cross-section of the resonator falls within the range accessible with the detection electronics used. While the temperature and pressure measurements this close to T_λ are not precise enough to compare the scattering corrections determined from this plot with those made at lower temperatures, the scattering corrections for the circumferential modes and the onset of the depth modes are identical at $n=1.16$. It is also possible that finite-size effects might be a factor this close to the λ point. This measurement indicates that the Al_2O_3 superleak is homogeneous and isotropic.

Figure 15 is a similar broad-band plot for the Grafoil superleak. In this case, high temperatures were not necessary in order to make the depth mode onset observable. The scattering correction determined for the depth mode is $n=5.5\pm0.2$, significantly different from the $n=4.4$ for the circumferential mode. This difference is consistent with the picture of the Grafoil as microscopic plates roughly oriented parallel to the plane of the annulus. The pathway for the sound waves is even more tortuous for the depth modes than it is for the circumferential mode. This is due to the flow of the superfluid parallel and perpendicular to the graphite platelets. As was the case for the Al_2O_3 superleak, the acoustic spectrum is quite distinct above the depth mode onset with respect to its appearance below the onset. These facts, and the lack of any temperature or pressure dependence in the scattering correction show that the Grafoil superleak is homogeneous but anisotropic.

The resonator spectrum for the Grafoil foam superleak, shown in Fig. 16, displays no evidence of an onset for other resonance modes. Even assuming a scattering correction for the depth modes equal to the smallest scattering correction observed for the circumferential mode, the upper frequency of this plot is sufficiently high to encompass such a mode. While the spectrum becomes less clear with higher frequencies, the stronger response of the depth modes observed in the other superleaks is not a feature of this plot. This could be the result of a lack of uniform structural characteristics from region to region in the Grafoil foam. In any case, the observed behavior suggests the Grafoil foam superleak is both highly anisotropic and inhomogeneous.

ACKNOWLEDGMENT

This research was supported in part by National Science Foundation Grant Nos. DMR 8304371 and DMR 8701682, and the Office of Naval Research.

*Present address: The BDM Corporation, 7915 Jones Branch Drive, McLean, VA 22102-3396.

[1]Lord Rayleigh (J. W. Strutt), Philos. Mag. **47**, 375 (1899).
[2]Lord Rayleigh (J. W. Strutt), Philos. Mag. **34**, 481 (1892).
[3]B. B. Mandelbrot, *The Fractal Geometry of Nature* (Freeman, San Francisco, 1983).
[4]P. Sheng and R. Tao, Phys. Rev. B **31**, 6131 (1985).
[5]D. L. Johnson and P. N. Sen, in *Proceedings of Physics and Chemistry of Porous Media,* (Schlumberger-Doll Research, Ridgefield, Connecticutt), Proceedings of a Symposium on the

Physics and Chemistry of Porous Media, AIP Conf. Proc. No. 107, edited by D. L. Johnson and P. N. Sen (AIP, New York, 1984).
[6]P. L. Chow, W. E. Kohler, and G. C. Papanicolaou, *Multiple Scattering and Waves in Random Media* (North-Holland, New York, 1981).
[7]T. Ohtuski and T. Keyes, J. Phys. A **17**, L137 (1984).
[8]S. Feng, M. F. Thorpe, and E. Garbocai, Phys. Rev. B **31**, 276 (1965).
[9]P. Sheng, Phys. Rev. Lett. **95**, 60 (1980).
[10]S. He and J. D. Maynard, Phys. Rev. Lett. **57**, 3171 (1986).
[11]P. C. Hohenberg, in *Physics of Quantum Fluids*, edited by R. Kubo and F. Takano (Syokabo, Tokyo, 1971), p. 77.
[12]D. J. Bergman, B. J. Halperin, and P. C. Hohenberg, Phys. Rev. B **11**, 4253 (1975).
[13]D. L. Johnson and P. N. Sen, Phys. Rev. B **24**, 2486 (1981).
[14]A. W. Yanof and J. D. Reppy, Phys. Rev. Lett. **33**, 631 (1974).
[15]J. D. Maynard, Phys. Rev. Lett. **56**, 1156 (1986).
[16]P. N. Sen, W. C. Chew, and D. Wilkinson, in Ref. 5.
[17]E. Charlaix, E. Guyon, and N. Rivier, Solid State Commun. **50**, 999 (1984).
[18]D. L. Johnson, T. J. Plona, C. Scala, E. Pasierb, and H. Kojima, Phys. Rev. Lett. **49** (1982).
[19]J. B. Mehl and W. Zimmerman, Jr., Phys. Rev. Lett. **14**, 815 (1965).
[20]J. Rudnick, in *New Directions in Physical Acoustics*, Proceedings of the International School of Physics "Enrico Fermi," Course LVIII, Varenna, 1974, edited by D. Sette (North-Holland/Elsevier, New York, 1976), p. 112.
[21]M. Kriss and I. Rudnick, J. Low Temp. Phys. **3**, 339 (1970).
[22]E. H. Andrei and W. I. Glaberson, Phys. Rev. B **20**, 4447 (1979).
[23]S. Ramesh and J. D. Maynard, Phys. Rev. Lett. **49**, 47 (1982).
[24]S. Ramesh, Q. Zhang, G. Torzo, and J. D. Maynard, Phys. Rev. Lett. **52**, 2375 (1984).
[25]H. Kojima, W. Veith, S. J. Putterman, E. Guyon, and I. Rudnick, Phys. Rev. Lett. **27**, 714 (1971).
[26]H. Kojima, W. Veith, E. Guyon, and I. Rudnick, J. Low Temp. Phys. **25**, 195 (1976).
[27]P. Sheng and A. J. Callegari, Appl. Phys. Lett. **44**, 738 (1984).
[28]M. A. Biot, J. Acoust. Soc. Am. **28**, 168 (1956); **28**, 179 (1956).
[29]P. N. Sen and D. L. Johnson, Phys. Rev. B **27**, 3133 (1983).
[30]P. N. Sen, C. Scala, and M. Cohen, Geophys. **46**, 781 (1981).
[31]L. D. Landau and E. M. Lifshitz, *Fluid Mechanics* (Pergamon, Oxford, 1959), p. 31.
[32]Control Systems Research Division, Contraves Goerz Corporation, CSR Building, 632 Fort Duquesne Blvd. Pittsburgh, PA 15222.
[33]Winfred M. Berg, Inc., 499 Ocean Ave., East Rockaway, NY 11518.
[34]UCAR Grafoil, Carbon Products Division, Union Carbide Corporation, P. O. Box 6087, Cleveland, OH 44101.
[35]Linde Division of Union Carbide, Coatings Service Department, 1500 Polco Street, Indianapolis, IN 46224.
[36]J. Heiserman and I. Rudnick, J. Low Temp. Phys. **22**, 481 (1976).

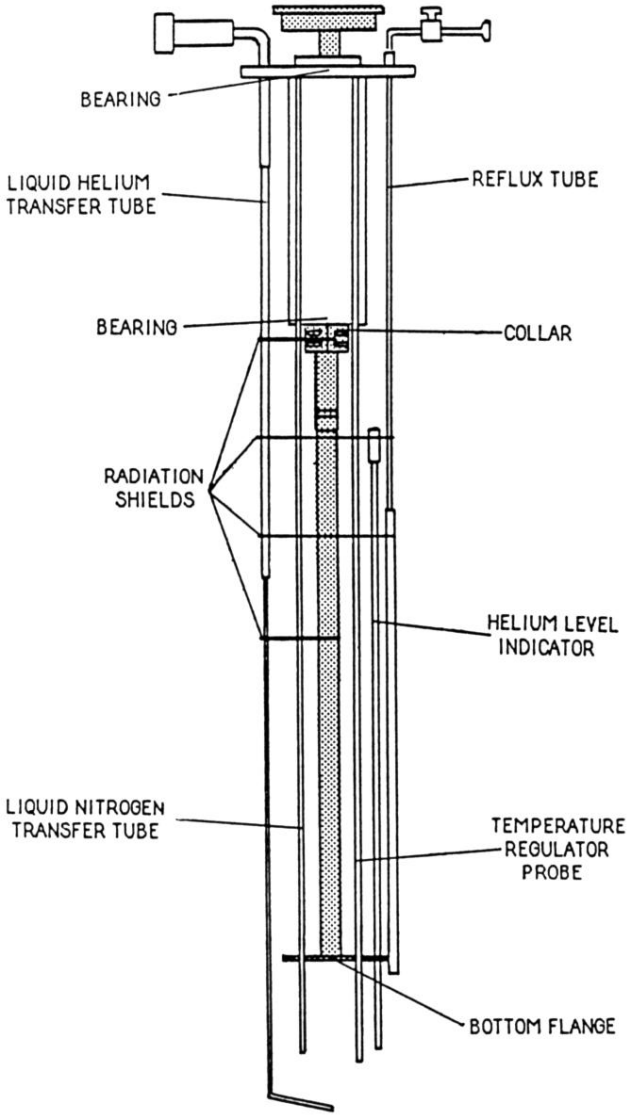

FIG. 1. Rotating cryostat insert.

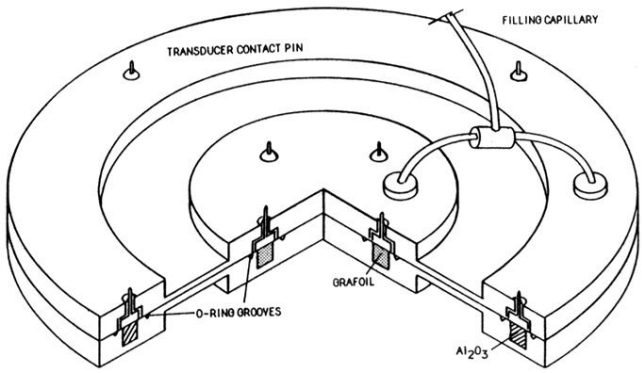

FIG. 3. Double annular acoustic resonators.